Science of the Total Environment 822 (2022) 153386

Contents lists available at ScienceDirect

Science of the Total Environment

journal homepage: www.elsevier.com/locate/scitotenv

Daytime and nighttime warming has no opposite effects on vegetation phenology and productivity in the northern hemisphere

Gaofeng Zhu [a,*,1], Xufeng Wang [b,*,1], Jingfeng Xiao [c,*,1], Kun Zhang [d], Yunquan Wang [e], Honglin He [f], Weide Li [g], Huiling Chen [a]

[a] Key Laboratory of Western China's Environmental Systems (Ministry of Education), Lanzhou University, 730000 Lanzhou, China
[b] Key Laboratory of Remote Sensing of Gansu Province, Heihe Remote Sensing Experimental Research Station, Northwest Institute of Eco-Environment and Resources, Chinese Academy of Sciences, 730000 Lanzhou, China
[c] Earth Systems Research Center, Institute for the Study of Earth, Oceans, and Space, University of New Hampshire, Durham, NH 03824, USA
[d] National Tibetan Plateau Data Center, Key Laboratory of Tibetan Environmental Changes and Land Surface Processes, Institute of Tibetan Plateau Research, Chinese Academy of Sciences, Beijing 100101, China
[e] School of Environmental Studies, China University of Geosciences, Wuhan 430074, China
[f] Key Laboratory of Ecosystem Network Observation and Modeling, Institute of Geographic Sciences and Natural Resources Research Chinese Academy of Sciences, Beijing 100101, China
[g] School of Mathematics and Statistics, Lanzhou University, Lanzhou 730000, Gansu, China

HIGHLIGHTS

- We settle the debate on the effects of day and night warming on vegetation activity.
- Misuse of methods lead to opposite effects of T_{max} and T_{min} on vegetation activity.
- Multicollinearity issue can be treated by properly choosing optimal ridge parameter.
- Asymmetric warming has no opposite effects on vegetation phenology and productivity.
- Improper handling of multicollinearity in regressions can cause misinterpretations.

GRAPHICAL ABSTRACT

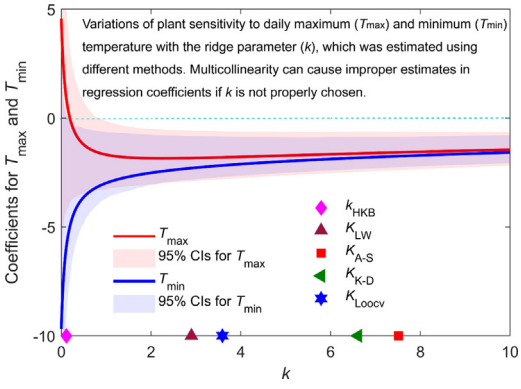

ARTICLE INFO

Article history:
Received 1 December 2021
Received in revised form 19 January 2022
Accepted 20 January 2022
Available online 29 January 2022

Editor: Elena Paoletti

Keywords:
Multicollinearity
Spring phenology
Autumn phenology

ABSTRACT

Over the past 50 years, global land surface air temperature has been rising at a much higher rate at night than during the day. Understanding plant responses to the asymmetric daytime and nighttime warming in the context of climate change has been a hot topic in global change biology and global ecology. It has been debatable whether the asymmetric warming has opposite effects on vegetation activity (e.g., phenology, productivity). Here we settle the debate by scrutinizing the underpinnings of different statistical methods and revealing how the misuse or improper use of these methods could mischaracterize the effects of asymmetric warming with in situ and satellite observations. The use of the ordinary least square (OLS) methods including both daytime (T_{max}) and nighttime (T_{min}) temperature in the multiple regression models could overlook the multicollinearity problem and yield the misinterpretations that T_{max} and T_{min} had opposite effects on spring phenology, autumn phenology, gross primary production (GPP), and normalized difference vegetation index (NDVI). However, when the OLS methods were applied with T_{max} and T_{min} included in separate models or alternatively the ridge regression (RR) method with properly selected ridge parameter

* Corresponding authors.
E-mail addresses: zhugf@lzu.edu.cn (G. Zhu), wangxufeng@lzb.ac.cn (X. Wang), j.xiao@unh.edu (J. Xiao).
[1] These authors contributed to the work equally.

http://dx.doi.org/10.1016/j.scitotenv.2022.153386
0048-9697/

Asymmetric warming
Vegetation activity
Gross primary production

was used, the effects of T_{max} and T_{min} on vegetation activity were generally in the same direction. The use of the RR method with improperly selected ridge parameter could also mischaracterize the effects of asymmetric warming. Our findings show that daytime and nighttime warming has no opposite effects on vegetation phenology and productivity in the northern hemisphere, and properly dealing with the multicollinearity problem is critical for understanding the effects of asymmetric warming on vegetation activity.

1. Introduction

Warmer temperatures are believed to have substantial impacts on northern hemisphere vegetation (e.g., advancing spring phenology, delaying autumn phenology, enhancing plant productivity). Nevertheless, global land surface air temperature data show that over the past five decades nights have been warming much faster than days, and daily minimum temperatures (T_{min}) have increased about 40% faster than daily maximum temperatures (T_{max}) (Davy et al., 2017; Solomon, 2007). Moreover, climate projections suggest that the diurnal asymmetry in the global warming trend is likely to continue in many regions, particularly in the northern latitudes (IPCC, 2013). Understanding plant responses to the asymmetric warming is a key challenge in climate change and global change biology studies.

Many recent studies have examined the impacts of the asymmetric diurnal warming on vegetation activity (e.g., phenology, productivity) in the northern hemisphere (Cheesman and Winter, 2013; Peng et al., 2013; Xia et al., 2014; Piao et al., 2015; Fu et al., 2016; Rossi and Isabel, 2017; Shen et al., 2016; Tan et al., 2015; Wu et al., 2018; Chen et al., 2020). However, the direction (i.e., sign) of the impacts of daytime and nighttime warming on vegetation activity has been debatable. Some previous studies based on regression analyses suggested that asymmetric warming had opposite effects on vegetation activity, such as autumn phenology (Chen et al., 2020; Wu et al., 2018), carbon cycle (Xia et al., 2014) and vegetation productivity (Tan et al., 2015). These studies indicate that the influences of daytime and nighttime warming would offset each other, weakening the impacts of warming on vegetation activity. The opposite effects were not supported by recent field experiments on spring phenology (Fu et al., 2016; Rossi and Isabel, 2017), plant growth (Cheesman and Winter, 2013; Phillips et al., 2011), and respiration (Phillips et al., 2011). These field studies showed that daytime and nighttime warming may affect vegetation activity with different magnitude but in the same direction. These experiments indicate that daytime and nighttime warming would reinforce the effects of warming on vegetation activity with larger influences by daytime warming. Therefore, settling the debate is critical for understanding and projecting the responses of ecosystems to global warming.

Previous studies typically used multiple linear regression to examine plant responses to the asymmetric warming of T_{max} and T_{min} (Xia et al., 2014; Tan et al., 2015; Wu et al., 2018; Chen et al., 2020). In these studies, the response variable (e.g., phenology, productivity) was regressed against both T_{max} and T_{min} along with other climatic factors to quantify the relative effects of daytime and nighttime warming. However, T_{max} and T_{min} are typically highly correlated to each other, and including both temperature variables in the same regression model can lead to multicollinearity (Dormann et al., 2013). In this case, the ordinary-least-squares (OLS) methods that have been often used can yield unreliable temperature sensitivity estimates with even incorrect signs (Alin, 2010). The ridge regression (RR) method (Hoerl and Kennard, 1970) can overcome the multicollinearity issue and has also been used to investigate the relative effects of T_{max} and T_{min} on autumn phenology (Chen et al., 2020). However, improper estimates of temperature sensitivity with opposite signs may still occur if the ridge parameter is not correctly selected. Thus, one crucial issue with the research on the effects of the asymmetric warming on vegetation activity is whether the opposite effects of T_{max} and T_{min} derived from the regression analyses are only misinterpretations or mischaracterizations caused by the misuse or improper use of the statistical methods.

Here we elucidate whether asymmetric daytime and nighttime warming has opposite effects on vegetation phenology and productivity in the northern hemisphere by scrutinizing the underpinnings of different statistical approaches and properly using these methods. Specifically, the objectives of this study are to (*i*) identify the influences of different methods on the interpretations of the asymmetric warming effects on vegetation activity; (*ii*) investigate the effects of asymmetric warming on phenology and productivity and northern ecosystems; and (*iii*) settle the debate whether asymmetric warming has opposite effects on vegetation activity. In this study, both in situ and satellite-based observations of the start of growing season (SOS), the end of growing season (EOS), and vegetation productivity (i.e., gross primary production (GPP) or normalized difference vegetation index (NDVI)) were used to investigate the effects of asymmetric daytime and nighttime warming on northern vegetation activity.

2. Materials and methods

2.1. In-situ data

The FlUXNET2015 database (https://fluxnet.fluxdata.org/data/fluxnet2015-dataset/) was used to explore the effects of daytime and nighttime warming on SOS, EOS, and GPP at the ecosystem scale. We selected 56 sites that have at least 7 years of high-quality measurements from the database (Supplementary Table S1). SOS and EOS were extracted from the smoothed daily GPP curves, and the extraction of the phenology data was described in a previous study (Wang et al., 2019). Daily maximum temperature (T_{max}) and minimum temperature (T_{min}) were calculated from the half-hourly meteorological data in the FLUXNET2015 database, and then daily T_{max} and T_{min} were aggregated to monthly values. The preseason for SOS (EOS) was defined as the period from January (June) to the month which multiyear average SOS (EOS) is in. Preseason T_{max}, T_{min}, shortwave radiation, and precipitation were calculated for SOS and EOS, respectively. Growing season GPP was calculated as the sum of daily GPP over the period from SOS to EOS, and the growing season T_{max}, T_{min}, shortwave radiation, and precipitation were calculated for the same period.

2.2. Satellite-derived data

We used gridded SOS and EOS derived from a long-term satellite derived NDVI product: the GIMMS NDVI3g dataset during the period from 1982 to 2014. The derivation of SOS and EOS from the GIMMS NDVI3g dataset is described in a previous study (Wang et al., 2019). The GIMMS NDVI3g phenology product for the northern hemisphere (Wang et al., 2019) is available online at http://data.globalecology.unh.edu. The SOS and EOS estimates are ensemble means based on five widely used phenology extraction methods. The growing season average NDVI was calculated as the mean of monthly maximum composite from April to October in the northern hemisphere. To match the spatial resolution of the gridded climate data, the SOS, EOS and growing season average NDVI data were resampled to 0.5-degree spatial resolution. Satellite-derived NDVI has been widely used as a proxy for plant productivity in many studies (Xiao et al., 2019).

The MODIS phenology product (MCD12Q2v006) was also used to examine the effects of T_{max} and T_{min} on phenology. The MODIS phenology product was also resampled to the spatial resolution of 0.5 degree.

The MODIS land cover product with the International Geosphere-Biosphere Programme (IGBP) classification scheme was used to compare temperature sensitivity among different vegetation types. The IGBP classification scheme consists of 17 land cover types. Considering the flux site availability, seven vegetation types were used in this study: evergreen

needleleaf forests (ENF), deciduous broadleaf forests (DBF), mixed forests (MF), open shrublands (OSH), Grasslands (GRA), permanent wetlands (WET) and croplands (CRO).

2.3. Climate data

A long time series climate dataset - CRU-TS (Climatic Research Unit Time Series) 4.04 was used in this study (Harris et al., 2014). This dataset includes monthly maximum temperature (T_{max}), minimum temperature (T_{min}), precipitation, and cloud cover with a spatial resolution of 0.5 degree. The GRU-TS data for the period from 1982 to 2014 were downloaded from https://crudata.uea.ac.uk/cru/data. The SOS/EOS preseason T_{max}, T_{min}, precipitation and cloud cover were calculated for each pixel from the CRU-TS4.04 data with the same method as used for the FLUXNET2015 database.

2.4. Statistical analysis

To investigate the influences of statistical methods on the interpretation of the effects of T_{max} or T_{min} on vegetation activity (i.e., SOS, EOS, GPP, and NDVI), we performed three regression-type analyses with a varying number of independent variables (Eqs. (1)–(5)). According to the signs of regression coefficients, the sensitivities of vegetation activity to T_{max} and T_{min} were classified to four types: T^{+}_{max}/T^{-}_{min} (type A), T^{+}_{max}/T^{+}_{min} (type B), T^{-}_{max}/T^{+}_{min} (type C), and T^{+}_{max}/T^{-}_{min} (type D), where T^{+} and T^{-} represent the positive and negative sensitivities of vegetation activity to temperature, respectively.

We first used simple bivariate linear regression (two-variable) models expressed as follows:

$$y\tilde{\beta}_0 + \beta_1 \times T_{max} + \varepsilon \quad (1)$$

$$y\tilde{\beta}_0 + \beta_1 \times T_{min} + \varepsilon \quad (2)$$

where y is the response variable (i.e., SOS, EOS, or GPP), β_i ($i = 0, 1$) is the regression coefficient, ε is a random error component with a mean zero and an unknown variance σ^2, and T_{max} and T_{min} are the monthly maximum and minimum temperature (°C), respectively. The two-variable models include T_{max} and T_{min}, the two highly correlated variables, in separate models and thus are able to correctly reveal whether the sensitivity of vegetation activity to either variable is positive or negative.

We also used multiple linear regression models with four variables as follows:

$$y\tilde{\beta}_0 + \beta_1 \times P_r + \beta_2 \times SW + \beta_3 \times T_{max} + \varepsilon \quad (3)$$

$$y\tilde{\beta}_0 + \beta_1 \times P_r + \beta_2 \times SW + \beta_3 \times T_{min} + \varepsilon \quad (4)$$

where β_i ($i = 0, 1, 2$ and 3) is the regression coefficient, SW is the daily mean short-wave solar radiation (W m^{-2}), P_r is the cumulated precipitation during the study period (mm), and other notations have the same meanings as in Eqs. (1) and (2). Compared with the two-variable models, the four-variable models include T_{max} and T_{min} in separate models but include two other controlling factors – precipitation and solar radiation.

Besides two- and four-variable models, we also used the following multiple linear regression model with five variables:

$$y\tilde{\beta}_0 + \beta_1 \times P_r + \beta_2 \times SW + \beta_3 \times T_{max} + \beta_4 \times T_{min} + \varepsilon \quad (5)$$

where β_i ($i = 0, 1, \ldots, 4$) is the regression coefficient, and other notations have the same meanings as in Eq. (4). Generally, it is convenient to deal with multiple regression models in the matrix notation:

$$\boldsymbol{y} = \boldsymbol{X\beta} + \boldsymbol{\varepsilon} \quad (6)$$

where $\boldsymbol{y}$ is an $n \times 1$ vector of the response variables, $\mathbf{X}$ is an $n \times p$ matrix of the independent variable, $\boldsymbol{\beta}$ is a $p \times 1$ vector of regression coefficients, $\boldsymbol{\varepsilon}$ an $n \times 1$ vector of random errors, p is the number of independent variables, and n is the number of observations.

We first applied the ordinary least-squares (OLS) method, which was widely used in previous studies, to estimate the regression coefficients:

$$\beta = (\boldsymbol{X}'\boldsymbol{X})^{-1}\boldsymbol{X}'y \quad (7)$$

where $\boldsymbol{X}'$ is the transpose matrix of $\mathbf{X}$. The t-test was used to determine whether the regression coefficient is statistically significant. Noticeably, the regression coefficient is the same as the correlation coefficient if the data are standardized (Keith, 2019). We used the variance inflation factor (VIF) to diagnose the multicollinearity between the independent variables, and the value of VIF for the lth independent variable is calculated as (Marquaridt, 1970):

$$VIF_l = \frac{1}{1-R_l^2} \quad (8)$$

where $R_l^2 (l = 1, 2, \ldots, p)$is the coefficient of multiple determination obtained from regressing x_l on the other regressor variables. Clearly, if x_l is nearly linearly dependent on some of the other regressors, then R_l^2 will be near unity and VIF_l will be large. In the absence of any linear relationship (orthogonal) between the predictor variables, R_l^2 would be zero and VIF_l would be one. The deviation of VIF_l from 1 indicates departure from orthogonality and tendency toward multicollinearity. Generally, VIFs lower than 3 indicate that the predictor variables are linearly independent, while VIFs larger than 5 or 10 imply serious problems with multicollinearity (Cohen et al., 2013; Keith, 2019).

When two or more independent variables in multiple regression models are highly correlated (i.e., Eq. (5)), the problem of multicollinearity occurs (Supplementary A1). We then used the ridge regression (RR) method to solve the regression models. Specifically, the RR method solves the matrix inverse problem by adding a nonzero value of k (ridge or shrinkage parameter) to the diagonal elements of $\boldsymbol{X'X}$ so that the ridge estimator for the linear coefficients is expressed as (Hoerl and Kennard, 1970):

$$\beta = (\boldsymbol{X}'\boldsymbol{X} + k\boldsymbol{I}_n)^{-1}\boldsymbol{X}'y \quad (9)$$

where $\mathbf{I}_n$ is the identity matrix; and k is the ridge or shrinkage parameter, which determines the strength of the penalty imposed on regression coefficients. In this study, the optimal k was estimated using the leave-one-out cross-validation (LOOCV) method, which employs the entire dataset to calibrate the model and thus can obtain unbiased regression coefficient estimations (James et al., 2013). In this method, the regression coefficients were estimated using all observations except for one single data point which is used to calculate the test squared error (TSE) between the model prediction and the observation. The procedure is repeated n times until every observation is used exactly once for calculating the TSE. The mean squared error (MSE) for a given k is calculated as the average of these n TSEs. Then, the optimal value of k is chosen as the one for which the MSE is minimal across all MSE values. Other methods in selecting the optimal ridge parameter (k) used in previous studies were also used for comparison with the LOOCV method (Supplementary A2). To assess the statistical significance of the ridge regression coefficients, we used 2000 bootstrap samples with replacement from the original data and fitted the model to the samples using the RR method. The values between 2.5 and 97.5 percentiles of the ridge regression coefficients were considered as the 95% confidence intervals. If the intervals do not include 0, the regression coefficients are significantly different from 0. On the contrary, if the intervals include 0, we could not reject the null hypothesis that the ridge regression coefficients are 0. To evaluate the reduction of multicollinearity by the RR method, the VIF of the lth ($l = 1, 2, \ldots, p$) independent variable for each value of k is computed using the lth diagonal element of the matrix (Ryan, 2008):

$$d = (\boldsymbol{X}'\boldsymbol{X} + kI_n)^{-1}\boldsymbol{X}'\boldsymbol{X}(\boldsymbol{X}'\boldsymbol{X} + kI_n)^{-1} \quad (10)$$

These analyses were mainly conducted based on in situ observations of SOS, EOS and GPP from the FLUXNET2015 database. We also used satellite-based observations of SOS and EOS to evaluate whether our findings based on in situ measurements would apply to every location across the northern hemisphere. The analyses based on both in situ and satellite observations were used to determine whether the asymmetric effects of daytime and nighttime warming on vegetation phenology and productivity were caused by improper use of statistical methods.

3. Results

3.1. Evidence from in situ observations

The simple bi-variate linear regressions (OLS) between SOS and T_{max} or T_{min} (two-variable models with only one of the two temperature variables included in each model; Eq. (1) and (2)) showed how T_{max} and T_{min} affected SOS separately. The majority of the FLUXNET sites (54 out of 56) fell in Type A (T^{-}_{max}/T^{-}_{min} with negative sensitivities to both T_{max} and T_{min}) and Type B (T^{+}_{max}/T^{+}_{min}, with positive sensitivities to both T_{max} and T_{min}) (Fig. 1a), and the sensitivity of SOS to T_{max} had the same sign as that to T_{min} (Fig. 1b). Similar results were obtained when we regressed SOS against precipitation, solar radiation, and T_{max} or precipitation, solar radiation, and T_{min} (four-variable models with only one of the two temperature variables included in each model; Eqs. (3) and (4)) (Supplementary Figs. S1 and S2). The values of the variance inflation factors (VIF) for the three independent variables in the multiple linear regressions were all significantly below the critical threshold (Supplementary Fig. S3a and b), and thus there were no multicollinearity problems in these models.

However, when we regressed SOS against both T_{max} and T_{min} along with precipitation and solar radiation (a five-variable model with both temperature variables included in the same model; Eq. (5)), substantially different results were obtained. The majority of the 54 sites fell within Type C (T^{-}_{max}/T^{+}_{min} with negative and positive sensitivities to T_{max} and T_{min}, respectively) and Type D (T^{+}_{max}/T^{-}_{min}, with positive and negative sensitivities to T_{max} and T_{min}, respectively) (Fig. 1c). The VIF values for T_{min} and T_{max} in the regression model were both above the critical threshold (Supplementary Fig. S3c) due to their high correlation ($R^2 = 0.88$, $p < 0.001$; Supplementary Fig. S4). This indicates the existence of multicollinearity in this model, which could lead to unreasonable interpretations about how asymmetric warming influenced vegetation activity (e.g., SOS responded oppositely to T_{max} and T_{min}, Fig. 1d). The sensitivities of SOS to T_{max} and T_{min} that were statistically significant also exhibited larger variations in magnitude, and varied from -45.2 days $^{\circ}C^{-1}$ to 87.4 days $^{\circ}C^{-1}$ for T_{max} and from -89.6 days $^{\circ}C^{-1}$–46.0 days $^{\circ}C^{-1}$ for T_{min} (Fig. 1b, Supplementary Table S2). These are typical mathematical artifacts of the OLS method when the multicollinearity problem exists in the model.

To corroborate our finding that the opposite effects of T_{max} and T_{min} on SOS were caused by the multicollinearity in the five-variable model based on the OLS method, we used the average daytime temperature (T_{day}) to replace T_{min} and regressed SOS simultaneously against precipitation, solar radiation, T_{max} and T_{day}. It is anticipated that the two daytime temperature measures (T_{max} and T_{day}) should have similar effects on SOS. Counterintuitively, however, this method shows that SOS responded oppositely to T_{max} and T_{day} (Supplementary Fig. S5e and f). Thus, the OLS methods with both temperature variables included in the same model, which were widely used in previous studies, could not properly reveal the

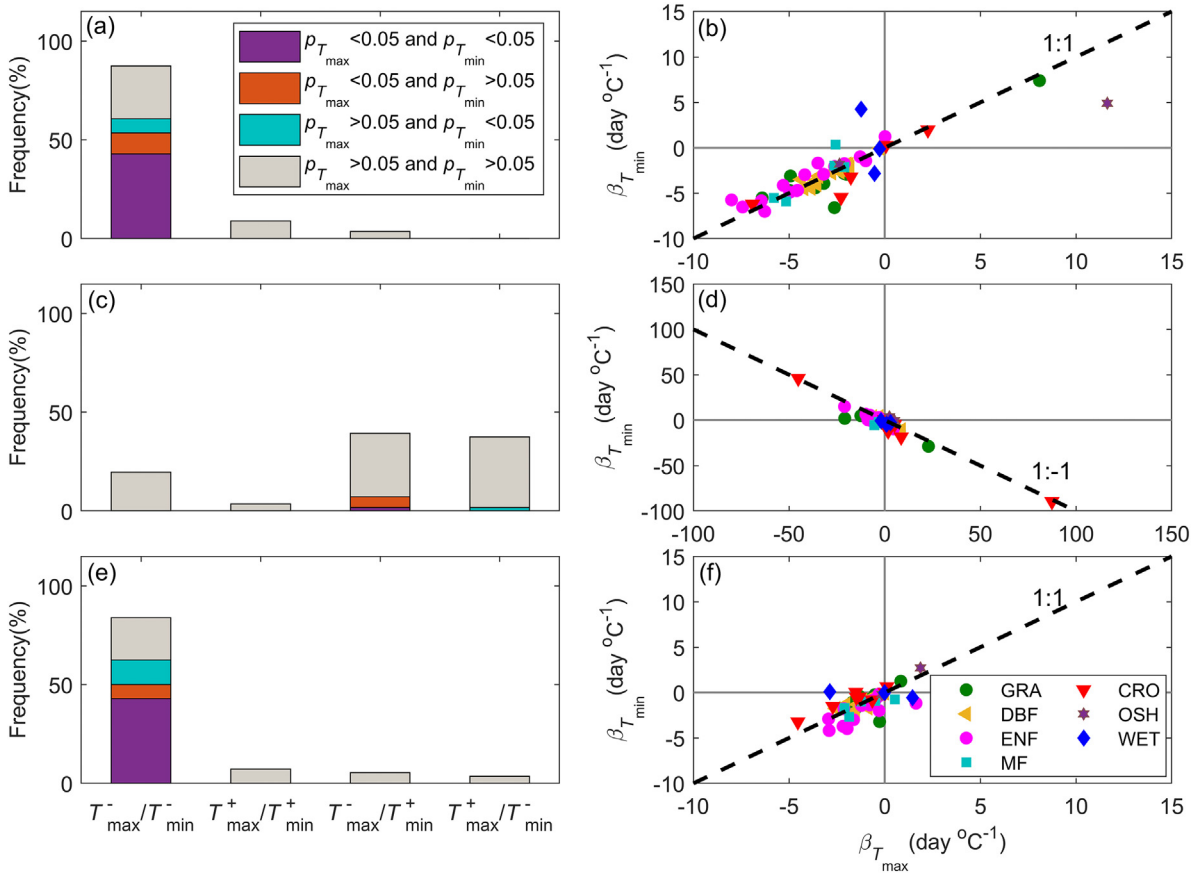

Fig. 1. Sensitivity of spring phenology (i.e., start of growing season, SOS) to daily maximum (T_{max}) and minimum (T_{min}) temperature from two- and five-variable OLS models and the five-variable RR model at FLUXNET sites. The frequency of the SOS sensitivity to T_{max} and T_{min} in T^{-}_{max}/T^{-}_{min} (Type A), T^{+}_{max}/T^{+}_{min} (Type B), T^{-}_{max}/T^{+}_{min} (Type C), and T^{+}_{max}/T^{-}_{min} (Type D) is shown in (a) (the two-variable OLS model), (c) (the five-variable OLS model), and (e) (five-variable RR model). The scatter plots between the SOS sensitivity to T_{max} and the SOS sensitivity to T_{min} for the two- and five-variable OLS models and the five-variable RR model are shown in (b), (d) and (f), respectively. Here, T^{+} and T^{-} represent the positive and negative sensitivities of SOS to temperature, respectively.

relative effects of daytime and nighttime warming on spring phenology due to the multicollinearity.

To overcome the problem of multicollinearity in the five-variable model (Eq. (5)), we tested the performance of the ridge regression (RR) method in estimating the sensitivity of SOS to T_{max} and T_{min} (Fig. 1e, f). The majority of the sites (54 out of 56) belonged to Type A (T^-_{max}/T^-_{min}), suggesting that with both temperature variables included in the same model and the use of the RR method, T_{max} and T_{min} had no opposite effects on SOS but both advanced SOS (Fig. 1e). This result is similar to that obtained by the OLS methods treating T_{max} and T_{min} separately (the two- and four-variable models; Fig. 1a, b, Supplementary Fig. S1) but not to that based on the five-variable OLS model (Fig. 1c, d).

For the two-variable model, the sensitivity values (i.e., regression coefficients) that were statistically significant ($p < 0.05$) for both T_{max} (36 out of 56) and T_{min} (32 out of 56) were only found within type A, suggesting that daytime and nighttime warming could advance the onset of spring phenology; on average, an increase of 1 °C in T_{max} or T_{min} would advance SOS by about 4 days (Fig. 2a). For the five-variable OLS model, only few sites had statistically significant ($p < 0.05$) sensitivity values for both T_{max} (6 out of 56; Fig. 2b) and T_{min} (4 out of 56; Fig. 2b) (Fig. 1g). For the five-variable RR model, the statistically significant ($p < 0.05$) sensitivity of SOS to T_{max} (28 out of 56; Fig. 2c) and T_{min} (31 out of 56; Fig. 2c) was only found in Type A (T^-_{max}/T^-_{min}) (Fig. 2c). Thus, both daytime and nighttime warming advanced SOS. The statistically significant T_{max} sensitivity varied from -3.98 to -0.66 days °C^{-1} with a median of -1.39 days °C^{-1}, and the T_{min} sensitivity ranged from -4.54 to -0.47 days °C^{-1} with a median of -1.32 day °C^{-1} (Fig. 2c). Interestingly, we found that the absolute magnitude of the significant sensitivities of SOS to T_{max} and T_{min} differed among sites (Supplementary Table S2 and Fig. S6), indicating that the effects of asymmetric warming on spring phenology were different for different ecosystems.

Unlike the OLS method (Figs. 1c, d; 2b), the RR method properly handled the multicollinearity in the five-variable model with both T_{max} and T_{min}, two highly correlated variables, included and thereby revealed that daytime and nighttime warming actually had no opposite effects on SOS. Despite its advantage, the RR method relies on the proper selection of the ridge parameter (k) for ensuring the performance of the method. The estimated ridge regression coefficients of T_{max} and T_{min} varied with k (Fig. 3a) (with one FLUXNET site shown as an example here). When $k = 0$, the RR model is equivalent to the five-variable OLS model (Eq. (5)). The regression coefficients for T_{max} and T_{min} had opposite signs when k was small (<1). As k further increased, the sign of the coefficient for T_{max} changed from positive to negative and eventually the coefficients for both T_{max} and T_{min} tended to stabilize. The optimal k value was estimated using the leave-one-out cross validation (LOOCV) strategy and other ridge parameter selection methods. Notably, the optimal k value selected by the HKB method was too small in this case. The optimal k value (~4) estimated using the LOOCV method was reasonable because both T_{max} and T_{min} stabilized as negative values (Fig. 3b). Similar patterns of ridge regression coefficients with the changes in k were observed at other FLUXNET sites.

Besides SOS, we also investigated the influences of the different methods on interpretations of asymmetric warming effects on EOS (Supplementary Figs. S7 and S8) and GPP for the FLUXNET sites (Supplementary Figs. S9 and S10). Similarly, when both T_{max} and T_{min} were included in the regression equation, the OLS methods indicated that T_{max} and T_{min} had opposite effects on EOS and GPP. These were also caused by

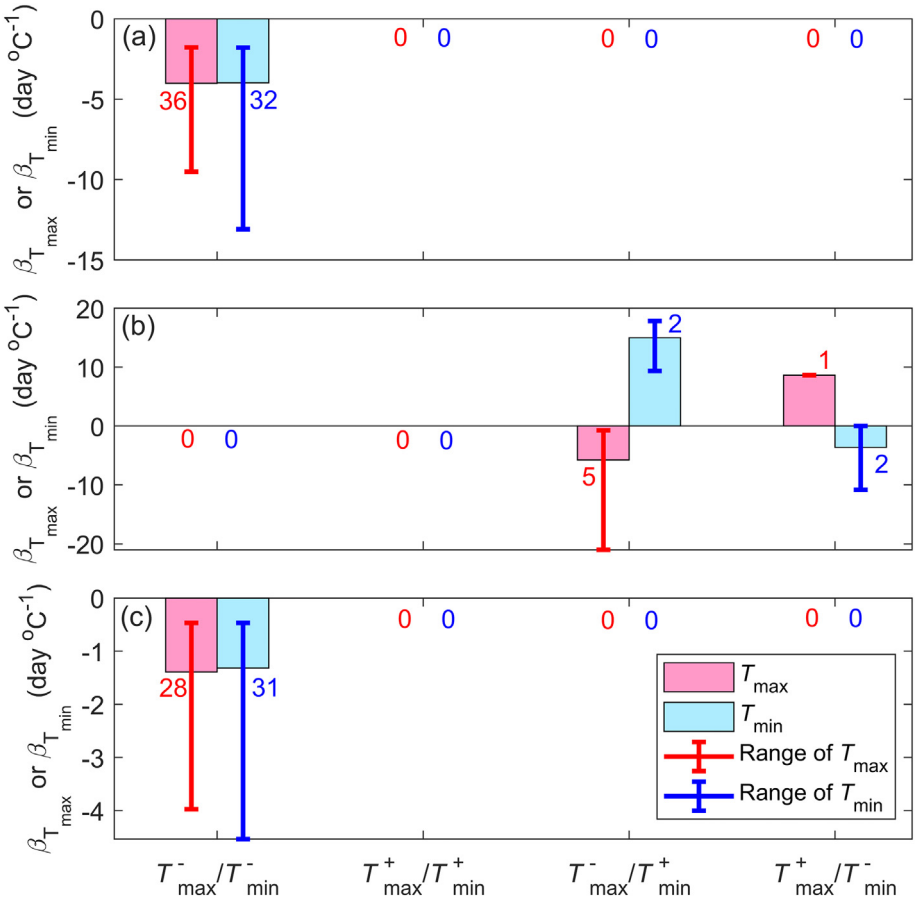

Fig. 2. The number of FLUXNET sites for different types of sensitivity of spring phenology (i.e., start of growing season, SOS) to daily maximum (T_{max}) and minimum (T_{min}) temperature (Type A: T^-_{max}/T^-_{min}; Type B: T^+_{max}/T^+_{min}; Type C: T^-_{max}/T^+_{min}; Type D: T^+_{max}/T^-_{min}). The models included are: (a) the two-variable OLS model, (b) the five-variable OLS model, and (c) the five-variable RR model. Each number within the plots shows the number of sites that have statistically significant T_{max} or T_{min} sensitivities to spring phenology. T^+ and T^- represent the positive and negative sensitivities of SOS to temperature, respectively.

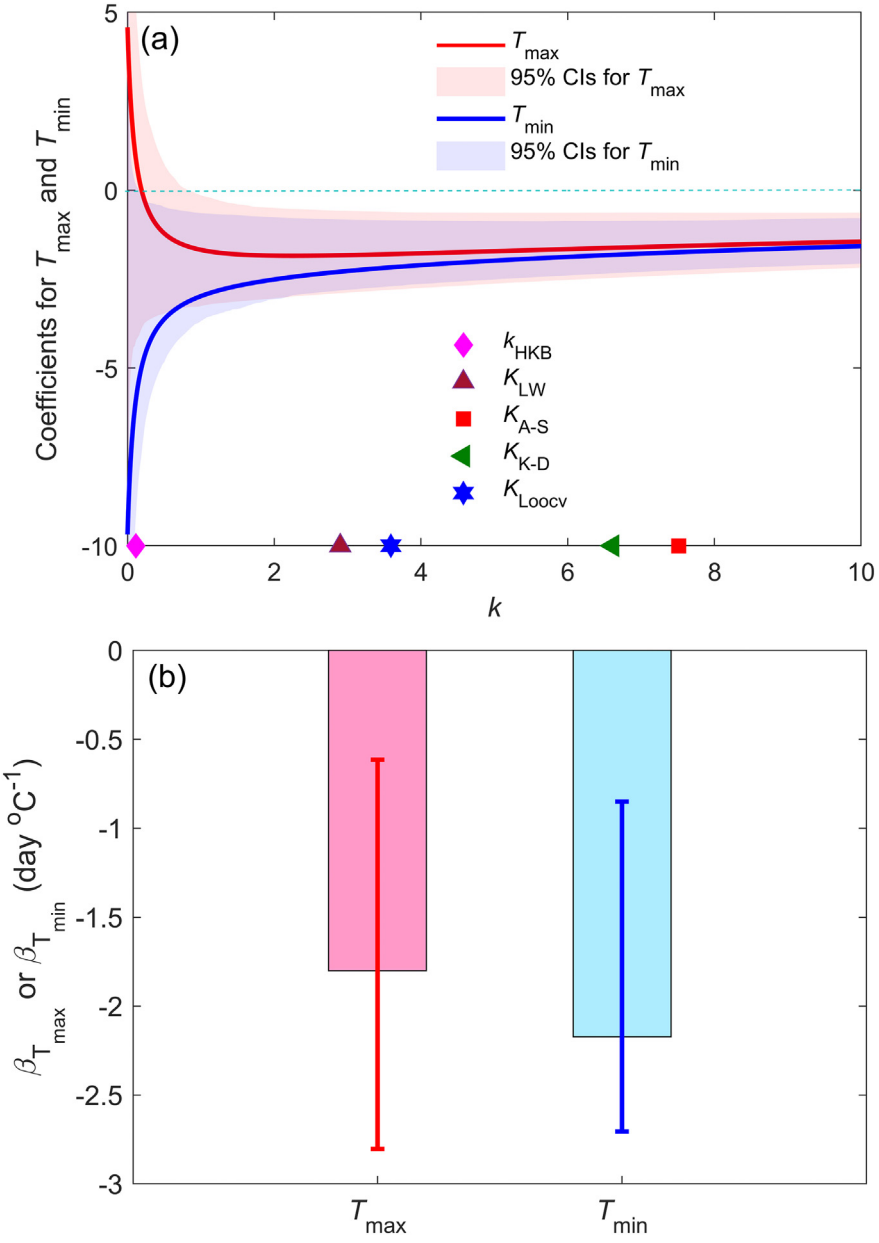

Fig. 3. Sensitivity of spring phenology (i.e., start of growing season, SOS) to daily maximum (T_{max}) and minimum (T_{min}) temperature based on the ridge regression (RR) method. (a) The regression coefficients (*the solid lines*) vary with the ridge parameter (k) at the selected FLXUNET site (CA-Man). The symbols indicate optimal k values estimated using the leave-one-out cross validation (LOOCV) strategy and other ridge parameter selecting methods (HKB, LW, A-S, K-D; See Supplementary A2 for details). We also selected 1000 bootstrap samples of our data to assess the statistical significance of the ridge regression coefficients. (b) The estimated SOS sensitivity to T_{max} and T_{min} at the selected FLXUNET site. The bar plot shows the median values for T_{max} (red) and T_{min} (blue) of the 1000 bootstrap samples of our data at the optimal k value, and the error bar stands for the 95% confidence intervals (CIs) of these values. The 95% CIs of T_{max} and T_{min} did not include 0, and the regression coefficient at the selected site were significantly different from 0. (For interpretation of the references to colour in this figure legend, the reader is referred to the web version of this article.)

multicollinearity due to the high correlation between T_{max} and T_{min} (Supplementary Fig. S11). In contrast, no opposite effects of T_{max} and T_{min} on EOS (Supplementary Figs. S7 and S8) and GPP (Supplementary Figs. S9 and S10) were found when the OLS methods were used by including T_{max} and T_{min} in separate models, or the RR method was used by choosing the proper k values.

The results of the RR method showed that both daytime and nighttime warming delayed EOS, and the mean sensitivity of EOS to T_{min} (2.08 ± 2.15 day °C^{-1}) was twice as large as that to T_{max} (1.10 ± 1.01 day °C^{-1}) (Supplementary Fig. S8d). This indicates that the autumn phenology might respond more strongly to nighttime warming than to daytime warming. GPP also responded to T_{max} and T_{min} in the same direction, and the increases in T_{max} and T_{min} may both enhance or depress GPP across different ecosystems (Supplementary Fig. S10d). Moreover, the mean positive sensitivity of GPP to T_{min} (16.6 ± 8.72 gC °C^{-1}) was slightly higher than that to T_{max} (14.0 ± 8.67 gC °C^{-1}), while the mean negative sensitivity of GPP to T_{min} (−19.4 ± 6.69 gC °C^{-1}) was almost identical with that to T_{max} (−19.5 ± 8.32 gC °C^{-1}) (Supplementary Fig. S10d).

3.2. Evidence from satellite observations

To evaluate the generality of our findings based on in situ measurements, we analyzed the effects of T_{max} and T_{min} changes on satellite-derived SOS in the northern hemisphere (>30° N). The results based on the satellite SOS data derived from the GIMMS NDVI3g product for the period 1982–2014 were consistent with those for the FLUXNET sites (Fig. 4).

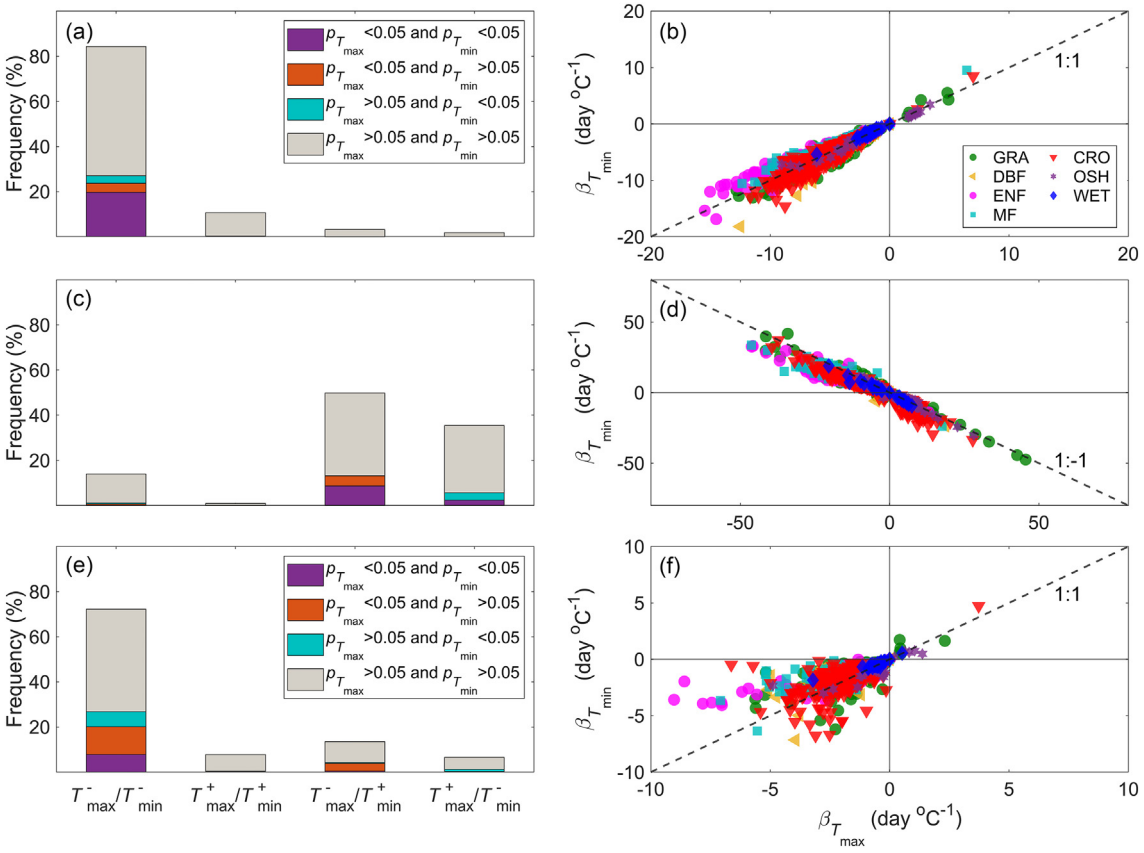

Fig. 4. Sensitivity of SOS derived from satellite observations to T_{max} and T_{min} estimated using the two- and five-variable OLS models and the five-variable RR model. The frequency of the SOS sensitivity to T_{max} and T_{min} in T^-_{max}/T^-_{min} (Type A), T^+_{max}/T^+_{min} (Type B), T^-_{max}/T^+_{min} (Type C), and T^+_{max}/T^-_{min} (Type D) is shown in (a) (the two-variable OLS model), (c) (the five-variable OLS model), and (e) (the five-variable RR model). The scatterplots between the SOS sensitivity to T_{max} and the SOS sensitivity to T_{min} for the two- and five-variable OLS models and the five-variable RR model are shown in (b), (d), and (f), respectively. T^+ and T^- represent the positive and negative sensitivities of SOS to temperature, respectively.

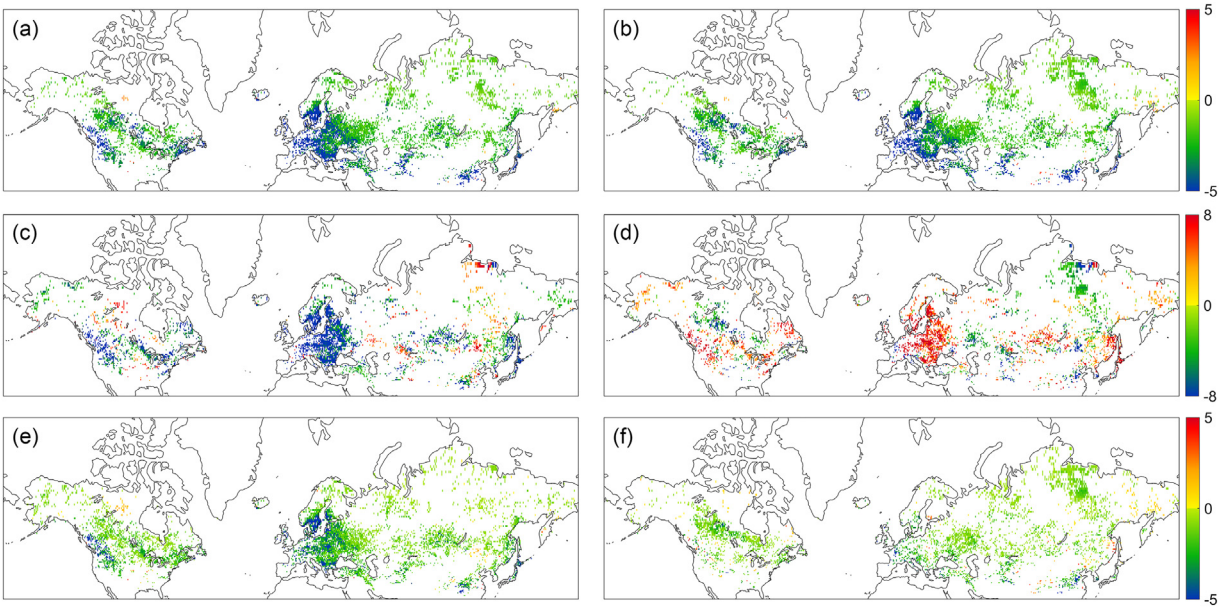

Fig. 5. Spatial distributions of the sensitivity of SOS derived from satellite observations (GIMMS NDVI3g) to T_{max} and T_{min} estimated using the two- and five-variable OLS models and the five-variable RR model. The sensitivity of SOS to T_{max} was estimated by the two-variable OLS model (a), the five-variable OLS model (c), and the five-variable RR model (e). The sensitivity of SOS to T_{min} was estimated by the two-variable OLS model (b), the five-variable OLS model (d), and the five-variable RR model (f). Pixels that were not vegetated or had insignificant sensitivity to T_{max} or T_{min} were masked out.

Notably, most of the pixels in the northern hemisphere fell within Types A (T^{-}_{max}/T^{-}_{min}) and B (T^{+}_{max}/T^{+}_{min}) for the OLS method by regressing SOS against T_{max} and T_{min} separately (95%; Fig. 4a) and the five-variable RR method (80%; Fig. 4e), and SOS responded to T_{max} and T_{min} in the same direction (Fig. 4b, f). In contrast, the five-variable OLS method indicated that when both T_{max} and T_{min} were included in the regression equation, most pixels (85%) belonged to Types C (T^{-}_{max}/T^{+}_{min}) and D (T^{+}_{max}/T^{-}_{min}) (Fig. 4c), leading to the mischaracterization that SOS responded oppositely to T_{max} and T_{min} (Fig. 4d). Also, the estimated sensitivity of SOS to T_{max} and T_{min} for the OLS method by treating T_{max} and T_{min} simultaneously showed large variations (−53.0 to 43.7 day °C^{-1}; Fig. 4b), which were generally beyond the reasonable ranges. These were mainly caused by the high correlations between T_{max} and T_{min} and prevailing multicollinearity over the study areas (Supplementary Fig. S12a and b).

The satellite-derived SOS product also allowed us to evaluate the spatial patterns of SOS changes in response to variations in T_{max} and T_{min} (Fig. 5). The results from the OLS methods by treating T_{max} and T_{min} separately (Fig. 5a, b) show that both daytime and nighttime warming advanced spring phenology in most areas of the northern hemisphere. In contrast, the five-variable OLS method led to consistently opposite effects from T_{max} and T_{min} on SOS in most areas of the northern hemisphere (Fig. 5c, d) due to the prevailing multicollinearity (Supplementary Fig. S12a, b). By properly dealing with the multicollinearity problem, the five-variable RR method shows that both T_{max} and T_{min} advanced SOS in most areas of the northern hemisphere (Fig. 5e, f). Pixels having negative sensitivity of SOS to T_{max} (33%) were more widespread than those having negative sensitivity of SOS to T_{min} (19%) in the northern middle latitudes (Supplementary Table S3). Also, the mean sensitivity of SOS to T_{max} (−1.55 ± 1.22 day °C^{-1}) was larger than that to T_{min} (−1.29 ± 1.08 day °C^{-1}) in absolute magnitude (Supplementary Table S3). These results indicate that the SOS in these areas was more efficiently triggered by T_{max} than by T_{min}. In the boreal areas, the fraction of the pixels having negative sensitivity of SOS to T_{max} was almost identical with that to T_{min} in both the percentage of the land area (10.5% and 10.4% for T_{max} and T_{min}, respectively) and in the magnitude (−0.72 ± 1.08 day °C^{-1} and −0.73 ± 0.72 day °C^{-1} for T_{max} and T_{min}, respectively) (Supplementary Table S3), indicating that daytime and nighttime warming had identical effects on SOS in these regions. We also examined the effects of asymmetric warming on SOS derived from MODIS for the period from 2001 to 2016. Similar results were obtained with the MODIS-based SOS (Supplementary Figs. S13 and S14).

We further investigated the influences of the different methods on the interpretations of the asymmetric warming effects on the satellite-derived EOS and NDVI derived from the GIMMS NDVI3g product for the period 1982–2014. Similarly, when both T_{max} and T_{min} were included in the regression equation, the OLS method led to the mischaracterization that EOS and NDVI responded oppositely to T_{max} and T_{min} (Figs. 6d and 7d) due to the high correlations between T_{max} and T_{min} (i.e., the multicollinearity problem) (Supplementary Fig. S12c-f). By contrast, no opposite effects of T_{max} and T_{min} on EOS and NDVI were found for the OLS method with T_{max} and T_{min} included in separate models (Figs. 6b and 7b) or for the RR method with the optimal k values properly selected (Figs. 6f and 7f).

In addition, we investigated the spatial variability of the sensitivities of EOS and NDVI to T_{max} and T_{min} based on the results derived from the five-variable RR method. Interestingly, some spatially contrasting effects of T_{max} and T_{min} on EOS were observed (Fig. 8e, f). In the northern middle latitudes, both T_{max} and T_{min} tended to delay EOS, and similar percentages of land areas (12.7% and 12.3% for T_{max} and T_{min}, respectively) had positive temperature sensitivities, but the mean sensitivity of EOS to T_{min} (1.0 ±

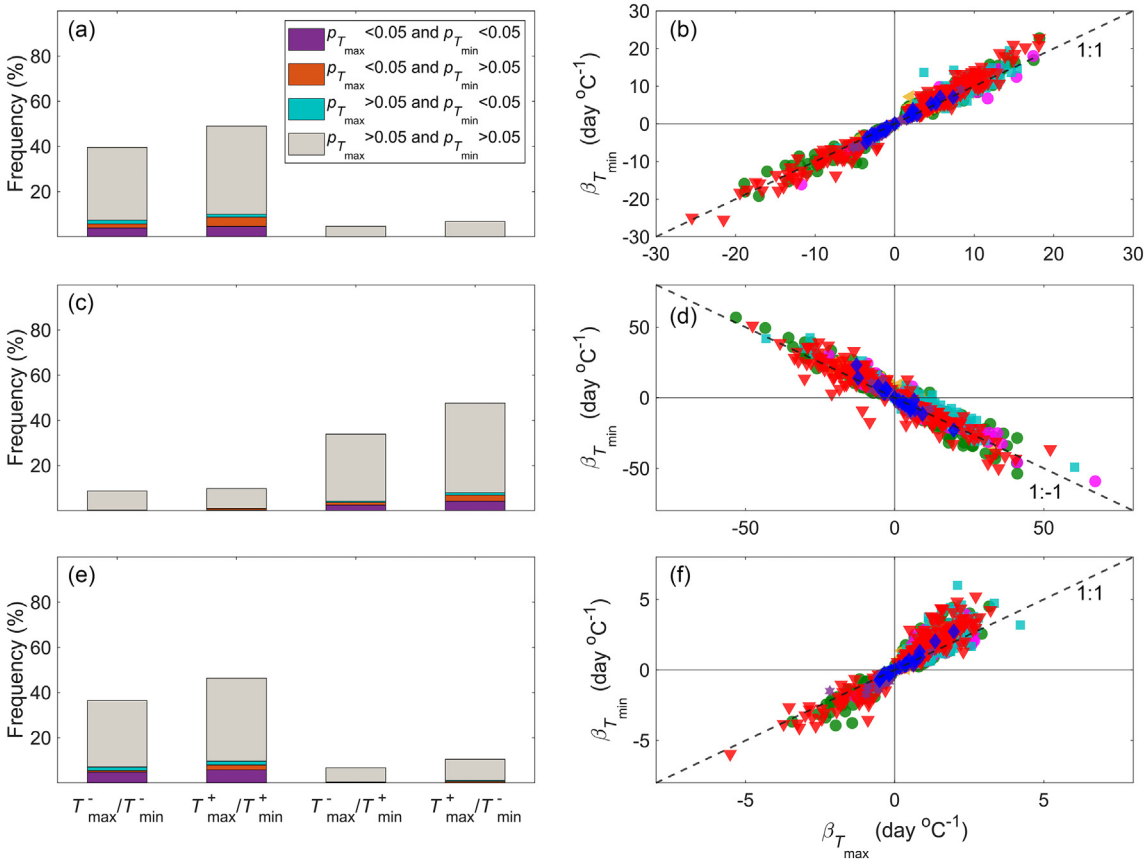

Fig. 6. Sensitivity of EOS derived from satellite observations to T_{max} and T_{min} estimated using the two- and five-variable OLS models and the five-variable RR model. The frequency of the SOS sensitivity to T_{max} and T_{min} in T^{-}_{max}/T^{-}_{min} (Type A), T^{+}_{max}/T^{+}_{min} (Type B), T^{-}_{max}/T^{+}_{min} (Type C), and T^{+}_{max}/T^{-}_{min} (Type D) are shown in (a) the two-variable OLS model, (c) the five-variable OLS model, and (e) the five-variable RR model. The scatter plots between the SOS sensitivity to T_{max} and the SOS sensitivity to T_{min} for two-, five-variable OLS models and the five-variable RR model are shown in (b), (d), and (f), respectively.

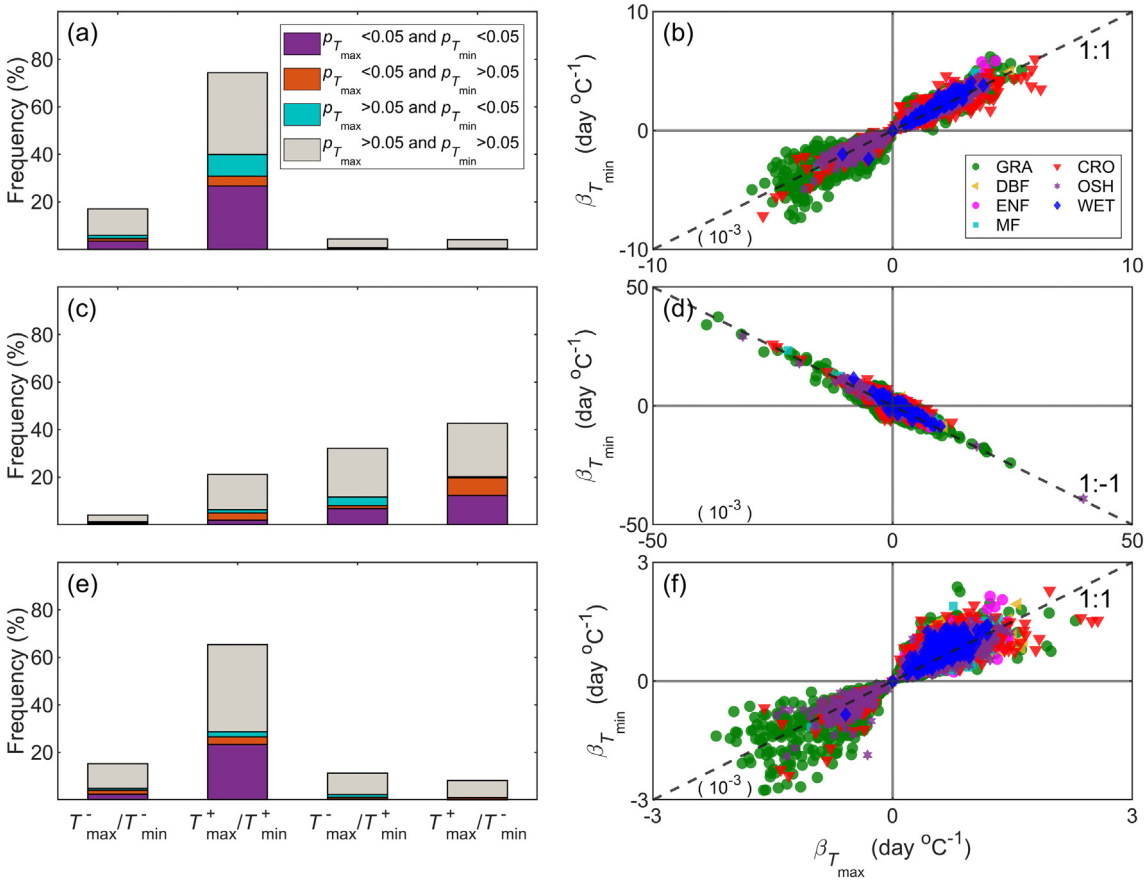

Fig. 7. Sensitivity of NDVI derived from satellite observations to T_{max} and T_{min} estimated using the two- and five-variable OLS models and the five-variable RR model. The frequency of the SOS sensitivity to T_{max} and T_{min} in T^-_{max}/T^-_{min} (Type A), T^+_{max}/T^+_{min} (Type B), T^-_{max}/T^+_{min} (Type C), and T^+_{max}/T^-_{min} (Type D) are shown in (a) the two-variable OLS model, (c) the five-variable OLS model, and (e) the five-variable RR model. The scatter plots between the SOS sensitivity to T_{max} and the SOS sensitivity to T_{min} for two-, five-variable OLS models and the five-variable RR model are shown in (b), (d), and (f), respectively.

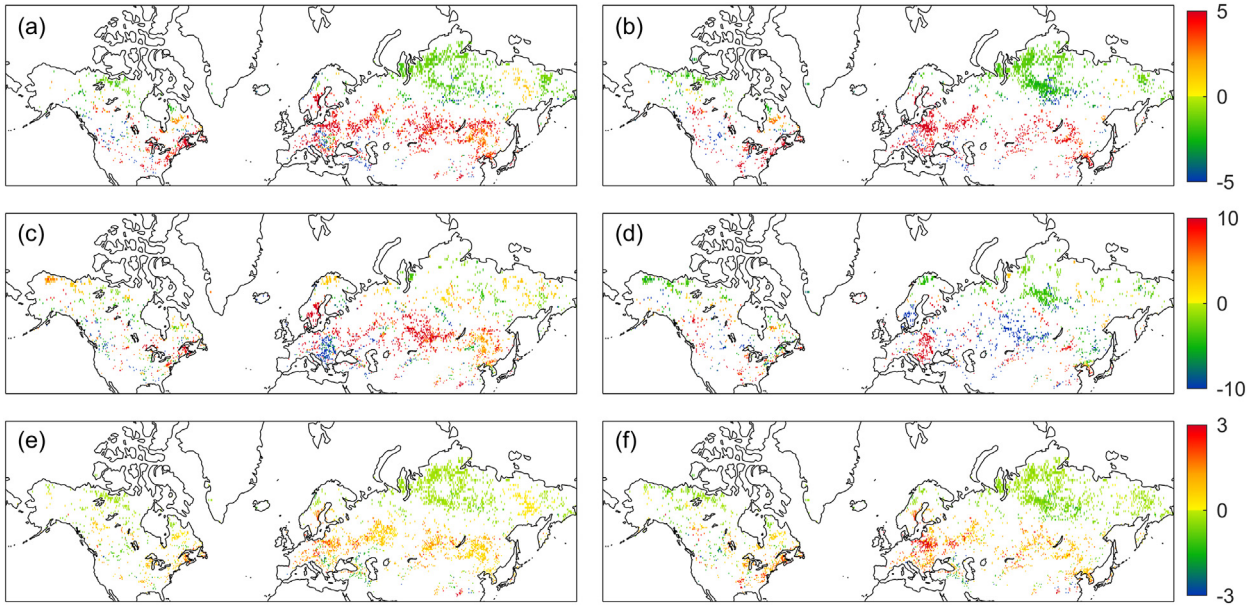

Fig. 8. Spatial distributions of the significant sensitivities of EOS derived from satellite observations to T_{max} and T_{min} estimated using the two- and five-variable OLS models and the five-variable RR model: spatial distributions of the statistically significant sensitivities of SOS to T_{max} obtained by the two-variable OLS model (a), the five-variable OLS model (c), and the five-variable RR model (e); spatial distributions of the statistically significant sensitivities of SOS to T_{min} obtained by the two-variable OLS model (b), the five-variable OLS model (d), and the five-variable RR model (f).

1.05 day °C^{-1}) was higher than that to T_{max} (0.76 ± 0.75 day °C^{-1}) (Supplementary Table S4). These results were consistent with those observed from in situ data as most FLUXNET sites were located in the middle latitudes. In contrast, both daytime and nighttime warming tended to advance EOS in the boreal regions. The pixels with negative EOS sensitivity to T_{min} accounted for a slightly larger fraction of the boreal regions than those with negative EOS sensitivity to T_{max} (13.7% and 10.6% of the land area for T_{min} and T_{max}, respectively); the mean EOS sensitivity to T_{min} (−0.32 ± 0.28 day °C^{-1}) was also larger than that to T_{max} (−0.23 ± 0.20 day °C^{-1}) (Supplementary Table S4), indicating that T_{min} had higher influence on EOS than T_{max} in these regions (Fig. 9).

The results based on the five-model RR method showed that both daytime and nighttime warming enhanced NDVI in boreal regions (Fig. 9e, f). The pixels with positive effects of T_{max} on NDVI (50.7%) accounted for almost the same fraction of the land area as those with positive effects of T_{min} on NDVI (47.8%), while the mean sensitivity of NDVI to T_{max} (5.31 ± 2.15% °C^{-1}) was much higher than that to T_{min} (2.15 ± 2.48% °C^{-1}) (Supplementary Table S5). Some spatially contrasting effects of T_{max} and T_{min} on NDVI were observed in the northern middle latitudes. For example, both T_{max} and T_{min} depressed NDVI in drier temperate regions (e.g., central Eurasia, western China, and western USA) both enhanced NDVI in wet regions (Supplementary Table S5).

4. Discussion

Based on both in situ and satellite observations, our study showed that the OLS method with both T_{max} and T_{min} included in one regression model led to the misconception that daytime and nighttime warming had opposite effects on vegetation activity (e.g., SOS, EOS, GPP, or NDVI) due to the high correlations between these two temperature variables. Multicollinearity, which refers to the linear relationship among two or more independent variables, is a common feature in regression analyses of many descriptive ecological data sets (Alin, 2010). Mathematically, no matter what the dependent variable (e.g., the various metrics used in this study) is, the OLS estimation equation becomes ill-conditioned if two or more independent variables are linearly related (Theorem in Supplementary A1). Under such conditions, unreasonable interpretations would be derived by using the OLS methods (Phillips et al., 2011). Thus, it is critical to ensure that the independent variables are unrelated in the multiple regression statistical models for the use of the OLS methods. The opposite effects of daytime and nighttime warming on vegetation activity reported in previous studies (Xia et al., 2014; Tan et al., 2015; Wu et al., 2018; Chen et al., 2020) were likely caused by the misuse or improper usage of the statistical methods. Moreover, the ill-conditioned OLS equations are highly sensitive to observation errors and can become unstable with minor changes in the input data (Cohen et al., 2013). Thus, the estimated sensitivities of vegetation activity to T_{max} and T_{min} based on the OLS method exhibited large variations and may be beyond the reasonable ranges (Fig. 1; Supplementary Figs. S7 and S9).

To overcome the multicollinearity problem, we applied the RR method and compared its performance against that of the OLS method with T_{max} and T_{min} included in separate models. The consistent findings between them illustrated that the RR method is a useful tool in solving the multicollinearity problem by decreasing the VIF values of correlated independent variables (Supplementary Table S2). These results showed that responses of vegetation activity to T_{max} and T_{min} were in the same direction. Compared with the OLS method by treating T_{max} and T_{min} separately, the RR method has an advantage in that it can quantify the relative influences of T_{min} and T_{max} on vegetation activity.

Despite the advantages of the RR method, the optimal ridge parameter (k) is usually unknown and needs to be properly estimated from data. To date, several quantitative methods have been proposed to select the optimal k value (Dorugade, 2014). Here, we compared the performances of different methods for the estimation of k in dealing with the multicollinearity problem of asymmetric warming (Supplementary A2 and Table S2). The optimal k values selected by the method proposed by Hoerl et al. (1975) (hereafter referred as the HKB method) were too small in some cases and could lead to improper estimates of sensitivity (i.e., regression coefficients) to vegetation activity, particularly GPP (Supplementary Table S2). Ryan (2008) also pointed that the HKB method is not proper for the extreme multicollinearity problems. The methods proposed by Alkhamisi and Shukur (2007) (A-S method) and Dorugade (2014) (A-D method) tended to overestimate the ridge parameter (Fig. 3a; Supplementary Table S2). Generally, the ridge parameter values selected by the method proposed by Lawless and Wang (1976) (L-W method) and the LOOCV method were reasonable (Supplementary Table S2). To use the RR method, it is critical to check

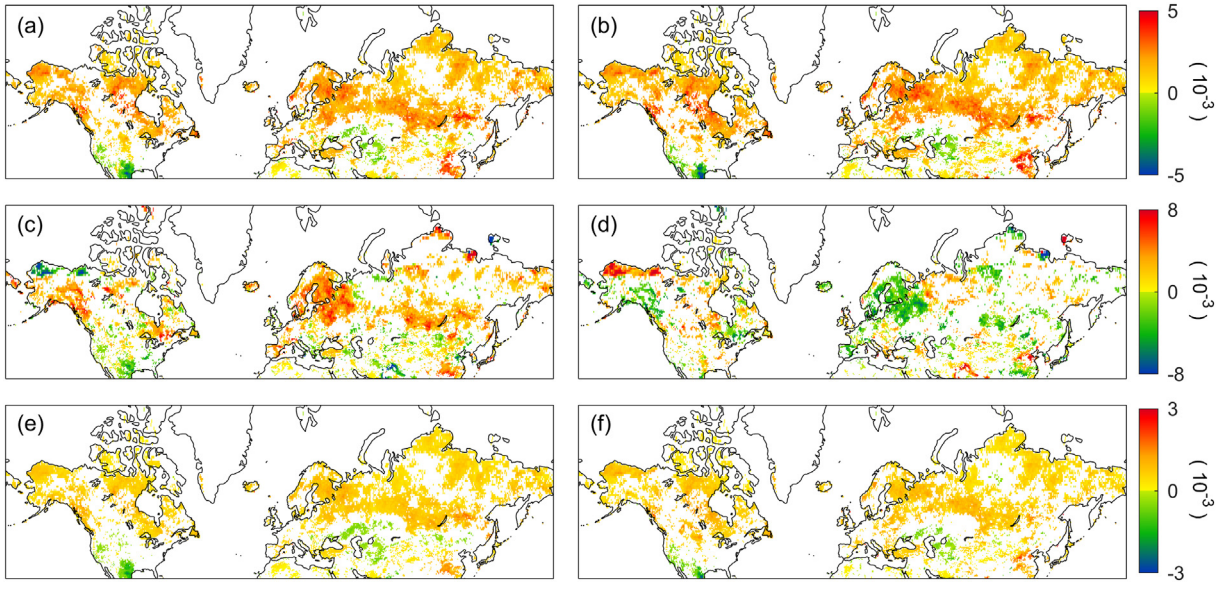

Fig. 9. Spatial distributions of the significant sensitivities of NDVI derived from satellite observations to T_{max} and T_{min} estimated using the two- and five-variable OLS models and the five-variable RR model: spatial distributions of the statistically significant sensitivities of SOS to T_{max} obtained by the two-variable OLS model (a), the five-variable OLS model (c), and the five-variable RR model (e); spatial distributions of the statistically significant sensitivities of SOS to T_{min} obtained by the two-variable OLS model (b), the five-variable OLS model (d), and the five-variable RR model (f).

the ridge trace (Fig. 3a) to ensure that the regression coefficients are stable at the selected k value because no method can lead to universally optimum k values (Cule and De Iorio, 2012). When counterintuitive results are obtained, the ridge trace (Fig. 3a) should be examined to ensure that the regression coefficients stabilize at the selected optimal ridge parameter.

Our finding that vegetation activity (i.e., SOS, EOS, GPP, and NDVI) responded to asymmetric daytime and nighttime warming in the same direction is consistent with results from manipulative experiments. Our results indicated that T_{max} and T_{min} could both enhance or reduce GPP. When water is readily available, increasing T_{max} and T_{min} can increase GPP (Manunta and Kirkham, 1996). This may be explained by the following mechanisms. First, photosynthesis in C3 plants generally has a lower temperature optimum than respiration (Luo et al., 2009), and therefore warming in the daytime (e.g., early morning) could result in more photosynthetic gains than respiratory costs (Dhakhwa and Campbell, 1998; Zheng et al., 2009). Second, nighttime plant respiration is highly related to carbon substrate from daytime photosynthesis. Some experiments reported that nighttime warming may stimulate compensatory photosynthesis due to depletion of leaf carbohydrates at night (Turnbull et al., 2002; Wan et al., 2009). Third, vegetation may acclimate to temperature warming and reduce respiration sensitivity to temperature (Armstrong et al., 2006; Atkin and Tjoelker, 2003; Cheesman and Winter, 2013; Phillips et al., 2011). In contrast, in water limited regions, both daytime and nighttime warming can strengthen water stress and thereby limit vegetation activity, and thus increases in T_{max} and T_{min} may have negative effects on ecosystem production in arid regions.

Our results also show that although vegetation activity responded to daytime and nighttime warming in the same direction, the sensitivities of vegetation activity to T_{max} and T_{min} could differ in magnitude. For example, both in situ and satellite data showed that the sensitivity of SOS to T_{min} was slightly lower than that to T_{max} in absolute magnitude, while the sensitivity of EOS to T_{min} was twice as large as that to T_{max}. Meanwhile, nights have been warming about 40% faster than days (Davy et al., 2017; Solomon, 2007), and the diurnal asymmetry in the global warming trend is projected to continue in the northern latitudes (IPCC, 2013). Therefore, nighttime warming could have larger effects on phenology particularly EOS than daytime warming. Our analysis based on the RR method revealed that both daytime and nighttime warming advanced the bud break in temperate tree species, and the impact of T_{max} was larger than that of T_{min}. These results were consistent with the findings of some previous studies (Piao et al., 2015; Fu et al., 2016; Rossi and Isabel, 2017). However, the impact of T_{max} on SOS was lower than or equal to that of T_{min} at some biomes (Fig. 2b-e), especially in the boreal regions of North America and eastern Siberia (Fig. 3c and f). This is mainly because the plants in boreal regions use the photoperiodism to protect them from the risk of freezing damage. As the photoperiod is equally long in autumn and spring, plants generally break dormancy by experiencing a dose of low temperatures (Körner and Basler, 2010). T_{min} can also limit soil root water absorption through soil frozen in cold regions (Pangtey et al., 1990), and affect plant growth in spring. Thus, T_{min} may play a more or equally important role in controlling SOS than T_{max} in these regions. Daytime and nighttime warming can both advance or both delay leaf senescence, partly due to water availability in autumn across different regions and ecosystems. To date, however, there still is a lack of such experiments on direct effects of asymmetric warming on autumn phenology and further experiments are needed.

Finally, our finding that vegetation activity responds to asymmetric warming in the same direction indicates that terrestrial biosphere models driven by the average daily temperature (e.g., LPJ-DGVM (Sitch et al., 2003), Biome-BGC (Thornton et al., 2002)) instead of sub-daily (e.g., hourly) data might be able to simulate the overall effects of warming on vegetation activity. However, these models implicitly assumed that the effects of T_{max} and T_{min} on vegetation activity are equal. Our results indicated that the sensitivities of vegetation activity to daytime and nighttime warming may be different, and meanwhile, nights warmer much faster than the days. Thus, these models could underestimate the effects of warmer temperatures.

5. Conclusions

To our knowledge, this is the first time to investigate how the improper use of statistical methods can mischaracterize the effects of asymmetrical daytime and nighttime warming on vegetation activity (e.g., phenology, productivity). Different methods may lead to different interpretations of the influences of asymmetrical warming on vegetation activity. Our results demonstrated that the opposite effects of T_{max} and T_{min} on vegetation activity interpreted by the OLS methods and reported in some previous studies are caused by the misuse or improper use of statistical methods. The RR method is a useful tool in dealing with the multicollinearity problem and quantifying the relative effects of daytime and nighttime warming, but properly choosing the optimal ridge parameter is critical for obtaining reasonable results. The optimal ridge parameter determined by the HKB method may be too small due to the extreme multicollinearity, and can cause improper estimates in regression coefficients. Proper usage of the statistical methods is critical for understanding the relative effects of asymmetric warming on northern hemisphere vegetation. Our findings can improve our understanding of how global warming will affect Earth's terrestrial ecosystems. Future well-designed field manipulative experiments are needed to better understand the mechanisms underlying the effects of asymmetric warming on plant phenology and growth under a changing climate.

CRediT authorship contribution statement

G.F.Z., X.F.W. and J.F.X. are co-first authors and contributed to the work equally. G.F.Z., X.F.W. and J.F.X. designed this study, analyzed the data, wrote and revised the manuscript. K.Z., Y.Q.W., H.L.H., W.D. L., and H.L.C. contributed to data analysis. All authors discussed and reviewed the manuscript.

Declaration of competing interest

The authors declare no competing interests.

Acknowledgments

This research was supported by the National Key Research and Development Program of China (Grant No. 2016YFC0500203), and National Natural Science Foundation of China (Grants No. 42071138 & 42171019). J.X. was supported by University of New Hampshire. We thank all the PIs and other research personnel of the FLUXNET sites for making the flux data available. This work used eddy covariance data acquired and shared by the FLUXNET community, including these networks: AmeriFlux, AfriFlux, AsiaFlux, CarboAfrica, CarboEuropeIP, CarboItaly, CarboMont, ChinaFlux, Fluxnet-Canada, GreenGrass, ICOS, KoFlux, LBA, NECC, OzFlux-TERN, TCOS-Siberia, and USCCC. We thank the anonymous reviewers for their constructive comments on our manuscript.

Data availability statement

The in-situ phenology and preseason meteorological data was calculated from FLUXNET2015, which is available from https://fluxnet.org/data/fluxnet2015-dataset/. The latest GIMMS NDVI is downloaded from https://climatedataguide.ucar.edu/. The phenology data from GIMMS NDVI3g is available from http://data.globalecology.unh.edu. The grided meteorological data CRU-TS4.04 in the northern hemisphere is from http://www.cru.uea.ac.uk/web/cru. MODIS phenology is available from https://lpdaac.usgs.gov/products/mcd12q2v006/.

Code availability statement

The code used for the regression analysis is available from the corresponding authors upon request.

Appendix A. Supplementary data

Supplementary data to this article can be found online at https://doi.org/10.1016/j.scitotenv.2022.153386.

References

Alin, A., 2010. Multicollinearity. 2, 370–374.

Alkhamisi, M.A., Shukur, G., 2007. A Monte Carlo study of recent ridge parameters. Commun. Stat. Simul. Comput. 36, 535–547.

Armstrong, A.F., Logan, D.C., Atkin, O.K., 2006. On the developmental dependence of leaf respiration: responses to short- and long-term changes in growth temperature. Am. J. Bot. 93, 1633–1639.

Atkin, O.K., Tjoelker, M.G., 2003. Thermal acclimation and the dynamic response of plant respiration to temperature. Trends Plant Sci. 8, 343–351.

Cheesman, A.W., Winter, K., 2013. Elevated night-time temperatures increase growth in seedlings of two tropical pioneer tree species. The New Phytologist 197, 1185–1192.

Chen, L., Hänninen, H., Rossi, S., Smith, N.G., Pau, S., Liu, Z., Feng, G., Gao, J., Liu, J., 2020. Leaf senescence exhibits stronger climatic responses during warm than during cold autumns. Nat. Clim. Chang. 10, 777–780.

Cohen, J., Cohen, P., West, S.G., Aiken, L.S., 2013. Applied Multiple Regression/Correlation Analysis for the Behavioral Sciences. Routledge.

Cule, E., De Iorio, M., 2012. A Semi-automatic Method to Guide the Choice of Ridge Parameter in Ridge Regression arXiv preprint arXiv:1205.0686.

Davy, R., Esau, I., Chernokulsky, A., Outten, S., Zilitinkevich, S., 2017. Diurnal asymmetry to the observed global warming. Int. J. Climatol. 37, 79–93.

Dhakhwa, G.B., Campbell, C.L., 1998. Potential effects of differential day-night warming in global climate change on crop production. Clim. Chang. 40, 647–667.

Dormann, C.F., Elith, J., Bacher, S., Buchmann, C., Carl, G., Carré, G., Marquéz, J.R.G., Gruber, B., Lafourcade, B., Leitão, P.J., Münkemüller, T., McClean, C., Osborne, P.E., Reineking, B., Schröder, B., Skidmore, A.K., Zurell, D., Lautenbach, S., 2013. Collinearity: a review of methods to deal with it and a simulation study evaluating their performance. Ecography 36, 27–46.

Dorugade, A.V., 2014. New ridge parameters for ridge regression. J. Assoc. Arab Univ. Basic Appl. Sci. 15, 94–99.

Fu, Y.H., Liu, Y., Boeck, H.J.D., Menzel, A., Nijs, I., Peaucelle, M., Peñuelas, J., Piao, S., Janssens, I.A., 2016. Three times greater weight of daytime than of night-time temperature on leaf unfolding phenology in temperate trees. New Phytol. 212, 590–597.

Harris, I., Jones, P.D., Osborn, T.J., Lister, D.H., 2014. Updated high-resolution grids of monthly climatic observations – the CRU TS3.10 dataset. Int. J. Climatol. 34, 623–642.

Hoerl, A.E., Kennard, R.W., 1970. Ridge regression: biased estimation for nonorthogonal problems. Technometrics 12, 55–67.

Hoerl, A.E., Kannard, R.W., Baldwin, K.F., 1975. Ridge regression:some simulations.

IPCC, 2013. Observations: surface and atmospheric climate change. Climate Change 2013: The Physical Science Basis, Contribution of Working Group I to the Fourth Assessment Report of the IPCC. Cambridge University Press, Cambridge, UK and New York, NY, USA.

James, G., Witten, D., Hastie, T., Tibshirani, R., 2013. An Introduction to Statistical Learning: With Applications in R. Springer, New York.

Keith, T.Z., 2019. Multiple Regression and Beyond: An Introduction to Multiple Regression and Structural Equation Modeling. 3rd ed. Routledge, New York.

Körner, C., Basler, D., 2010. Phenology under global warming. Science 327, 1461–1462.

Lawless, J.F., Wang, P., 1976. A simulation study of ridge and other regression estimators. Commun. Stat. Theory Methods 5, 307–323.

Luo, Y., Sherry, R., Zhou, X., Wan, S., 2009. Terrestrial carbon-cycle feedback to climate warming: experimental evidence on plant regulation and impacts of biofuel feedstock harvest. Glob. Chang. Biol. Bioenergy 1, 62–74.

Manunta, P., Kirkham, M.B., 1996. Respiration and growth of sorghum and sunflower under predicted increased night temperatures1. J. Agron. Crop Sci. 176, 267–274.

Marquaridt, D.W., 1970. Generalized inverses, ridge regression, biased linear estimation, and nonlinear estimation. Technometrics 12, 591–612.

Pangtey, Y.P.S., Rawal, R.S., Bankoti, N.S., Samant, S.S., 1990. Phenology of high-altitude plants of kumaun in central himalaya, India. Int. J. Biometeorol. 34, 122–127.

Peng, S., Piao, S., Ciais, P., Myneni, R.B., Chen, A., Chevallier, F., Dolman, A.J., Janssens, I.A., Peñuelas, J., Zhang, G., Vicca, S., Wan, S., Wang, S., Zeng, H., 2013. Asymmetric effects of daytime and night-time warming on northern hemisphere vegetation. Nature 501, 88–92.

Phillips, C.L., Gregg, J.W., Wilson, J.K., 2011. Reduced diurnal temperature range does not change warming impacts on ecosystem carbon balance of Mediterranean grassland mesocosms. Glob. Chang. Biol. 17, 3263–3273.

Piao, S., Tan, J., Chen, A., Fu, Y.H., Ciais, P., Liu, Q., Janssens, I.A., Vicca, S., Zeng, Z., Jeong, S.-J., Li, Y., Myneni, R.B., Peng, S., Shen, M., Peñuelas, J., 2015. Leaf onset in the northern hemisphere triggered by daytime temperature. Nat. Commun. 6, 6911.

Rossi, S., Isabel, N., 2017. Bud break responds more strongly to daytime than night-time temperature under asymmetric experimental warming. Glob. Chang. Biol. 23, 446–454.

Ryan, T.P., 2008. Modern Regression Methods. John Wiley & Sons.

Shen, M., Piao, S., Chen, X., An, S., Fu, Y.H., Wang, S., Cong, N., Janssens, I.A., 2016. Strong impacts of daily minimum temperature on the green-up date and summer greenness of the tibetan plateau. Glob. Chang. Biol. 22, 3057–3066.

Sitch, S., Smith, B., Prentice, I.C., Arneth, A., Bondeau, A., Cramer, W., Kaplan, J.O., Levis, S., Lucht, W., Sykes, M.T., Thonicke, K., Venevsky, S., 2003. Evaluation of ecosystem dynamics, plant geography and terrestrial carbon cycling in the LPJ dynamic global vegetation model. Glob. Chang. Biol. 9, 161–185.

Solomon, S., 2007. Climate Change 2007: The Physical Science Basis. Contribution of Working Group I to the Fourth Assessment Report of the Intergovernmental Panel on Climate Change. Cambridge Univ. Press.

Tan, J., Piao, S., Chen, A., Zeng, Z., Ciais, P., Janssens, I.A., Mao, J., Myneni, R.B., Peng, S., Peñuelas, J., Shi, X., Vicca, S., 2015. Seasonally different response of photosynthetic activity to daytime and night-time warming in the northern hemisphere. Glob. Chang. Biol. 21, 377–387.

Thornton, P.E., Law, B.E., Gholz, H.L., Clark, K.L., Falge, E., Ellsworth, D.S., Goldstein, A.H., Monson, R.K., Hollinger, D., Falk, M., Chen, J., Sparks, J.P., 2002. Modeling and measuring the effects of disturbance history and climate on carbon and water budgets in evergreen needleleaf forests. Agric. For. Meteorol. 113, 185–222.

Turnbull, M.H., Murthy, R., Griffin, K.L., 2002. The relative impacts of daytime and night-time warming on photosynthetic capacity in Populus deltoides. Plant Cell Environ. 25, 1729–1737.

Wan, S., Xia, J., Liu, W., Niu, S., 2009. Photosynthetic overcompensation under nocturnal warming enhances grassland carbon sequestration. Ecology 90, 2700–2710.

Wang, X., Xiao, J., Li, X., Cheng, G., Ma, M., Zhu, G., Altaf Arain, M., Andrew Black, T., Jassal, R.S., 2019. No trends in spring and autumn phenology during the global warming hiatus. Nat. Commun. 10, 2389. https://doi.org/10.1038/s41467-019-10235-8.

Wu, C., Wang, X., Wang, H., Ciais, P., Peñuelas, J., Myneni, R.B., Desai, A.R., Gough, C.M., Gonsamo, A., Black, A.T., Jassal, R.S., Ju, W., Yuan, W., Fu, Y., Shen, M., Li, S., Liu, R., Chen, J.M., Ge, Q., 2018. Contrasting responses of autumn-leaf senescence to daytime and night-time warming. Nat. Clim. Chang. 8, 1092–1096.

Xia, J., Chen, J., Piao, S., Ciais, P., Luo, Y., Wan, S., 2014. Terrestrial carbon cycle affected by non-uniform climate warming. Nat. Geosci. 7, 173–180.

Xiao, J., Chevallier, F., Gomez, C., Guanter, L., Hicke, J.A., Huete, A.R., Ichii, K., Ni, W., Pang, Y., Rahman, A.F., Sun, G., Yuan, W., Zhang, L., Zhang, X., 2019. Remote sensing of the terrestrial carbon cycle: a review of advances over 50 years. Remote Sens. Environ. 233, 111383. https://doi.org/10.1016/j.rse.2019.111383.

Zheng, H., Chen, L., Han, X., 2009. The effects of global warming on soybean yields in a long-term fertilization experiment in Northeast China. J. Agric. Sci. 147, 11.